Fast inversion of Zeeman line profiles using central moments. II. Stokes V moments and determination of vector magnetic fields

P. Mein, H. Uitenbroek, N. Mein, V. Bommier, M. Faurobert

A&A 591, A64 (2016)
DOI: 10.1051/0004-6361/201525769

Astronomy & Astrophysics

Fast inversion of Zeeman line profiles using central moments

II. Stokes *V* moments and determination of vector magnetic fields

P. Mein[1], H. Uitenbroek[2], N. Mein[3], V. Bommier[1], and M. Faurobert[4]

[1] LESIA, Observatoire de Paris, PSL Research University, CNRS, Sorbonne Universités, UPMC Univ. Paris 06, Univ. Paris Diderot, Sorbonne Paris Cité, 5 place Jules Janssen, 92195 Meudon, France
e-mail: Pierre.Mein@obspm.fr
[2] National Solar Observatory, Sacramento Peak, PO Box 62, Sunspot, NM 88349, USA
[3] Observatoire de Paris, 5 place Jules Janssen, 92195 Meudon, France
[4] UMR 6525 H. Fizeau, Université de Nice Sophia Antipolis, CNRS, Observatoire de la Côte d'Azur, Campus Valrose, 06108 Nice, France

Received 30 January 2015 / Accepted 30 March 2016

ABSTRACT

Context. In the case of unresolved solar structures or stray light contamination, inversion techniques using four Stokes parameters of Zeeman profiles cannot disentangle the combined contributions of magnetic and nonmagnetic areas to the observed Stokes I.
Aims. In the framework of a two-component model atmosphere with filling factor f, we propose an inversion method restricting input data to Q , U, and V profiles, thus overcoming ambiguities from stray light and spatial mixing.
Methods. The V-moments inversion (VMI) method uses shifts S_V derived from moments of V-profiles and integrals of Q^2, U^2, and V^2 to determine the strength B and inclination ψ of a magnetic field vector through least-squares polynomial fits and with very few iterations. Moment calculations are optimized to reduce data noise effects. To specify the model atmosphere of the magnetic component, an additional parameter δ, deduced from the shape of V-profiles, is used to interpolate between expansions corresponding to two basic models.
Results. We perform inversions of HINODE SOT/SP data for inclination ranges $0 < \psi < 60°$ and $120 < \psi < 180°$ for the 630.2 nm Fe I line. A damping coefficient is fitted to take instrumental line broadening into account. We estimate errors from data noise. Magnetic field strengths and inclinations deduced from VMI inversion are compared with results from the inversion codes UNNOFIT and MERLIN.
Conclusions. The VMI inversion method is insensitive to the dependence of Stokes I profiles on the thermodynamic structure in nonmagnetic areas. In the range of Bf products larger than 200 G, mean field strengths exceed 1000 G and there is not a very significant departure from the UNNOFIT results because of differences between magnetic and nonmagnetic model atmospheres. Further improvements might include additional parameters deduced from the shape of Stokes V profiles and from large sets of 3D-MHD simulations, especially for unresolved magnetic flux tubes.

Key words. line: profiles – Sun: magnetic fields

1. Introduction

Most of the inversion techniques processing Zeeman line profiles derive magnetic field components and thermodynamical parameters from least-squares fits of $I \pm S$ profiles, where S represents the Stokes parameters Q, U, V successively. For weak fields, algorithms using central moments (Semel 1967; Uitenbroek 2003; Criscuoli et al. 2013) can provide measurements of magnetic field components. In a previous paper (Paper I; Mein et al. 2011), we extended the inversion by moment calculations of $I \pm S$ profiles to the general case of any magnetic field strength.

Stray light and unresolved structures. Zeeman line profiles can be disturbed by stray light effects from the atmosphere of the Earth, the telescope, and the spectrometer. To eliminate such effects, it was proposed to take neighbouring pixels or the quietest parts of the data set into account to correct the observed profiles in each solar point (Skumanich & Lites 1987; Orozco Suarez et al. 2007; Asensio Ramos 2009; Del Toro Iniesta et al. 2010).

If magnetic structures are unresolved, magnetic and nonmagnetic areas may contribute simultaneously to the same pixel. The more usual solution to this problem is to define a filling factor f and to assume that the contributions of the magnetic area to the Stokes parameters are If, Qf, Uf, and Vf, while the contribution of nonmagnetic areas is limited to the nonpolarized contribution $I'(1 - f)$. The intensities I and I' can be different. The ratio between areas of magnetic and nonmagnetic components is $f/(1 - f)$.

For unresolved magnetic structures, it is well known that products Bf can be measured more easily than B and f measured separately (Bommier et al. 2007). For two-component models with magnetic and nonmagnetic areas, independent measurements of f were proposed (Bommier et al. 2009; Bommier 2011) to deduce the magnetic strength B. In the special case of the quiet Sun, methods using two lines simultaneously with different Lande factors were used by Stenflo (1973, 2010). Complex three-component models have also been proposed with the MISMA code to take different models and different magnetic strengths into account (Viticchié et al. 2011; Viticchié & Sánchez Almeida 2011). Very low data noise levels are of course required to obtain accurate results with models that depend on many parameters.

New inversion code insensitive to nonmagnetic model atmosphere. In this paper, we propose an inversion method based on a two-component model using only the polarized parts of the profiles, independent of intensities I and I'. Magnetic strength B and inclination ψ are derived from moments of V-profiles and ratios of integrals of Q^2, U^2, and V^2. We do not investigate nearly transverse magnetic fields, but similar methods using Q-profiles might be developed for magnetic vector inclinations near 90°. We use moments of V-profiles to determine barycenters. These are very different from the moments used in Taylor expansions of absorption coefficients by Mathys & Stenflo (1987) and Solanki et al. (1987).

We begin with the definition of the observable quantities used in the V-moments inversion (VMI). We do not take into account the vector field azimuth ϕ, which might be deduced independently from Stokes Q and U and magneto-optical effects. In our simulations, at first we assume a given model atmosphere for magnetic areas. Later we propose a procedure to specify unknown models in the case of observations (Sect. 7).

We describe the inversion by deducing B and ψ from two quantities S_V and R_V, defined in Sect. 4. We derive polynomials necessary to extract B and ψ through a brief iteration process via synthetic spectra computed with the RH radiative transfer code (Uitenbroek 2001, 2003). We extend the method to the case of an unknown underlying solar model for the magnetic component using a third quantity D_V.

Coefficients of polynomials used in the inversion also depend on the instrumental broadening profile and, possibly, on unresolved transverse gradients of the magnetic field. We determine a broadening coefficient in the particuliar case of HINODE SOT/SP data and investigate expected data noise effects for standard models. We process data and compare results of VMI with maps deduced from inversions with UNNOFIT (Bommier et al. 2007) and the HAO MERLIN code (CSAC[1]).

2. The RH radiative transfer code

As in Paper I, we derive synthetic spectra of the 630.25 nm line with the RH radiative transfer code (Uitenbroek 2001, 2003), which is based on the multilevel accelerated lambda iteration scheme (Rybicki & Hummer 1991, 1992) to define the required polynomial coefficients for inversion. In the transfer solution, the coupled equations of statistical equilibrium and radiative transfer were solved for a 23-level, 33-line atomic model of Fe I, including the 630.25 and 630.15 nm lines. Non-LTE iterations were performed in the polarization free approximation to account for the effect of the splitting of the line profile on the radiative rates (Bruls & Trujillo Bueno 1996). More details can be found in Paper I.

We employed four different one-dimensional hydrostatic solar atmospheric models in the calculations: FALA, FALC, FALF (Fontenla et al. 1993), and MALTM (Maltby et al. 1986). These models represent a quiet cell interior, the averaged quiet sun, the solar network, and a sunspot umbra, respectively. To compute coefficients for the inversion process, we use synthetic profiles with small wavelength steps. However, to simulate noise effects on real observations (Sect. 10), we use synthetic profiles with the same spectral resolution as SOT/SP spectra (spectral step 2.147 pm). In all of the cases, we performed computation of moments used in the inversion process after profile interpolations by third degree spline functions.

[1] http://www.csac.hao.ucar.edu/

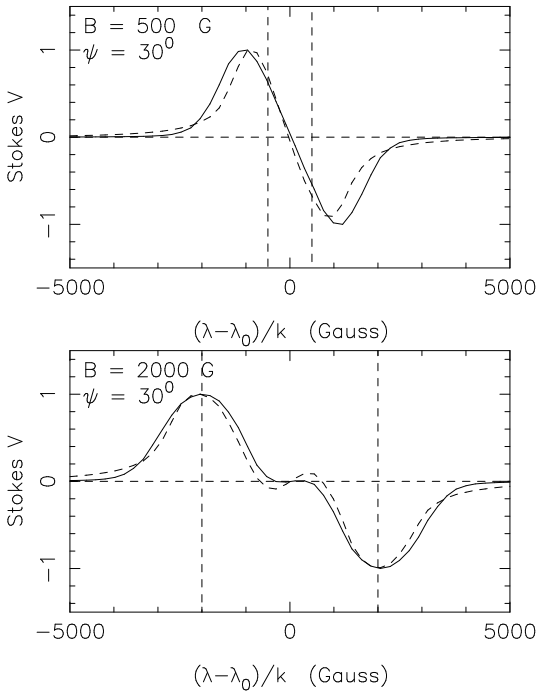

Fig. 1. V-profiles for FALC and MALTM models at disk center (full and dashed lines, respectively) with magnetic field strengths 500 G (*top*) and 2000 G (*bottom*). Profiles are scaled to their own maximum value.

3. *V*-profiles and vector magnetic field strength *B*

Figure 1 shows the V-profiles of the 630.25 nm line computed at disk center for FALC and MALTM models with magnetic field strengths B = 500 G and B = 2000 G (inclination ψ = 30°).

We denote with s the Zeeman splitting corresponding to the field strength B, for an effective Lande factor $\overline{g}$ and a line-center wavelength λ_0 as follows:

$$s = kB \tag{1}$$

with

$$k = 4.67 \times 10^{-12} \overline{g}\, \lambda_0^2, \tag{2}$$

where s and λ_0 are expressed in nm and B in Gauss.

In both cases, vertical dotted lines are drawn at wavelengths $\lambda = \lambda_0 + s$ and $\lambda = \lambda_0 - s$.

As expected, in the stronger field case (B = 2000 G), the two lobes of the V-profiles approximately coincide at the same positions as the dotted lines. This means that the field strength can be easily deduced from the shifts of the V-profiles alone. In the weaker field case (B = 500 G), however, the lobes are at larger distances than the dotted lines from line center and the distances depend on the width of the I profile and, thus, on the underlying corresponding atmosphere.

4. Inversion of *Q, U, V* profiles: Observable quantities S_V, R_V, and D_V

To deduce B and the inclination ψ from Stokes V, Q, and U profiles, we propose two observable quantities that are mainly sensitive to B and ψ, respectively.

The first quantity, S_V, is the half-shift between both lobes of the V^2-profile. We use V^2 instead of V to reduce the weights of line wings, which are very sensitive to data noise. We checked

that using V^2 instead of V significantly increases the accuracy of inversion results.

The second quantity, R_V, characterizes the ratio between integrals of $Q^2 + U^2$ and $V^2 + Q^2 + U^2$.

To specify the model atmosphere of magnetic areas inside each solar pixel, we use departures between the half-shift S'_V of V-profiles and the half-shift S_V of V^2-profiles that are sensitive to line wing shapes and noted as D_V.

We note that S_V, R_V, and D_V are very independent of global Doppler shifts of profiles.

4.1. Shift S_V and magnetic field strength B

In the following, moment calculations are performed with profiles interpolated by spline functions leading to a wavelength step divided by four with respect to the original spectral resolution.

Before calculating the half-shift S_V between the blue and red lobes of V^2-profiles, we must determine the central wavelength of the line. To take the possible asymmetry of profiles into account, we separately compute the moments of the positive and negative parts V_+ and V_- of the V-profile. V_+ and V_- are set to zero where V is negative and positive, respectively,

$$\lambda_0 = \left[\frac{\int_{-\infty}^{+\infty} V_+^2(\lambda)\lambda\,\mathrm{d}\lambda}{\int_{-\infty}^{+\infty} V_+^2(\lambda)\,\mathrm{d}\lambda} + \frac{\int_{-\infty}^{+\infty} V_-^2(\lambda)\lambda\,\mathrm{d}\lambda}{\int_{-\infty}^{+\infty} V_-^2(\lambda)\,\mathrm{d}\lambda} \right] \Big/ 2. \tag{3}$$

We have to compute central wavelengths λ_b and λ_r of the blue and red lobes. In the case of observed data, noise may strongly disturb moment calculations of $V^2(\lambda)$ because the mean signal is not zero in the far line wings. To avoid this problem, we keep the signal sign and we replace V^2 by $V \times |V|$ as follows:

$$\lambda_b = \frac{\int_{-\infty}^{\lambda_0} V(\lambda) \times |V(\lambda)|\lambda\,\mathrm{d}\lambda}{\int_{-\infty}^{\lambda_0} V(\lambda) \times |V(\lambda)|\,\mathrm{d}\lambda} \tag{4}$$

$$\lambda_r = \frac{\int_{\lambda_0}^{+\infty} V(\lambda) \times |V(\lambda)|\lambda\,\mathrm{d}\lambda}{\int_{\lambda_0}^{+\infty} V(\lambda) \times |V(\lambda)|\,\mathrm{d}\lambda}. \tag{5}$$

The shift S_V is half the wavelength distance between both converted into magnetic field units

$$S_V = 0.5(\lambda_r - \lambda_b)/k. \tag{6}$$

Figures 2a and 3a show theoretical values of S_V at disk center for different values of B and ψ for the FALC and MALTM models. The line styles depend on the values of ψ: full lines to 30° and dashed lines to 60°.

We can see that S_V depends mainly on B and slightly on ψ.

4.2. Ratio R_V and inclination angle ψ

In this section dealing with synthetic spectra, we consider ψ-values only between 0 and 90°. The extension to 180° is easily obtained for observed data, owing to the signs of the V-profile lobes.

The ratio of integrated $Q^2 + U^2$ and $Q^2 + U^2 + V^2$ profiles is 0 for $\psi = 0$ and 1 for $\psi = 90°$. It does not depend on the magnetic vector azimuth and can be used to determine the inclination. The use of the quantity R_V seems more convenient for forward polynomial inversion than the unlimited Q/V ratio used, for example, for quiet Sun analysis (Stenflo 2010).

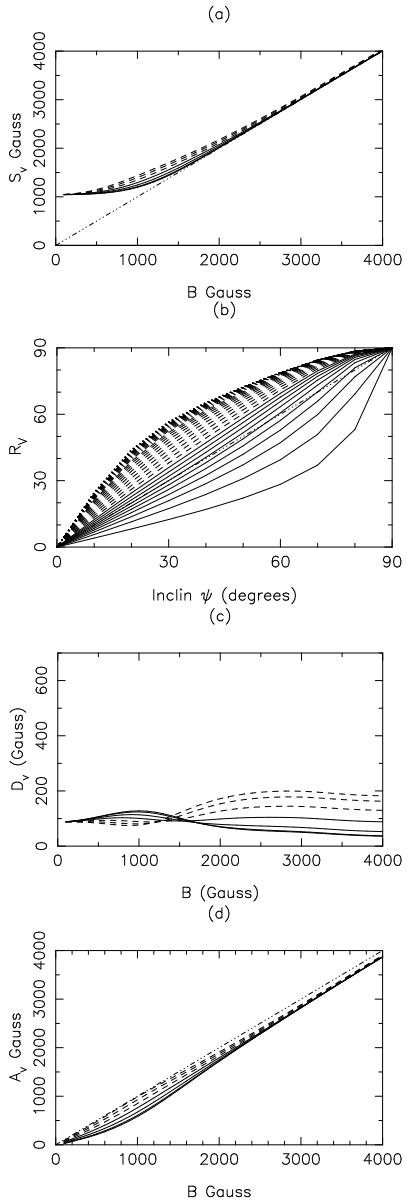

Fig. 2. S_V, R_V, D_V, and A_V functions for FALC model (Sect. 4).

We define the ratio R_V expressed in degrees and characterizing the inclination angle ψ through the equation

$$R_V = 90 \times \left[\frac{\int (Q^2(\lambda) + U^2(\lambda))\mathrm{d}\lambda}{\int (V^2(\lambda) + Q^2(\lambda) + U^2(\lambda))\mathrm{d}\lambda} \right]^{1/4}. \tag{7}$$

Figures 2b and 3b show theoretical values for FALC and MALTM models. R_V increases with ψ, regardless of the value of B. The line styles depend on the values of B: full lines from 100 G to 1000 G, dashed lines from 1100 G to 2000 G, dash-dotted from 2100 G to 3000 G, and dotted from 3100 G to 4000 G.

We note that data noise strongly affects values of R_V for small B for real observations. If we assume that noise levels are similar for Q, U, and V, the expected limit of R_V for zero magnetic strength is the high value

$$R_{V,\mathrm{lim}} = 90 \times (2/3)^{1/4} = 81.3°. \tag{8}$$

To reduce noise effects, we estimate noise in each solar point by the root mean square (RMS) of fluctuations in some wavelength

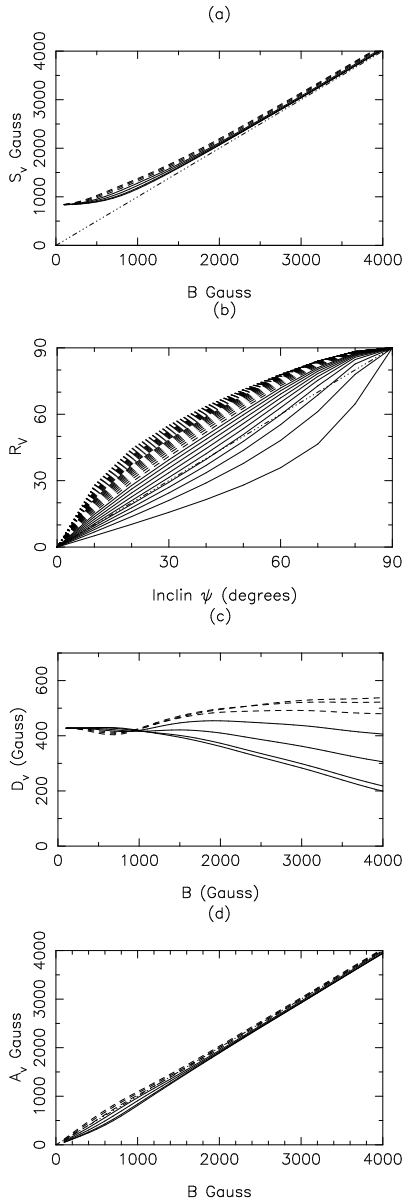

Fig. 3. S_V, A_V, R_V, and A_V functions for MALTM model.

points at the beginning and end of the available wavelength interval of the line. Then we subtract the result from the corresponding Q^2 and U^2 values. We do not modify V^2 to avoid undetermined R_V values. Results are shown in Sect. 10.

4.3. S'_V, D_V, and the model atmosphere

The difference between shifts S'_V of V-profiles and S_V of V^2-profiles, expressed in Gauss and named D_V, is used to specify the model atmosphere. The equations defining S'_V are very similar to Eqs. (4)−(6), i.e.,

$$\lambda'_b = \frac{\int_{-\infty}^{\lambda_0} V(\lambda)\lambda\,\mathrm{d}\lambda}{\int_{-\infty}^{\lambda_0} V(\lambda)\,\mathrm{d}\lambda} \tag{9}$$

$$\lambda'_r = \frac{\int_{\lambda_0}^{+\infty} V(\lambda)\lambda\,\mathrm{d}\lambda}{\int_{\lambda_0}^{+\infty} V(\lambda)\,\mathrm{d}\lambda} \tag{10}$$

$$S'_V = (\lambda'_r - \lambda'_b)/k \tag{11}$$

Figures 2c and 3c show theoretical values of

$$D_V = S'_V - S_V. \tag{12}$$

The line styles depend on the values of ψ: full lines to 30°, dashed lines to 60°.

5. A_V, a nearly linear function of B for a given model atmosphere

The function S_V is too far from a linear function of B to be approximated accurately by a polynomial with a small number of nonzero coefficients. If we call $S_{0,M}$ the limit at zero field of the function S_v relative to model M, we can define a new function,

$$A_V = (S_V^2 - S_{0,M}^2)^{1/2}, \tag{13}$$

which is nearly a linear function of B. Figures 2d and 3d show plots of A_V functions. Line styles are the same as in Fig. 2a.

6. Polynomials $P_A(A_V, \psi)$ and $P_R(R_V, B)$: inversion for a given model atmosphere

Because A_V is a monotonic function of B for all ψ values, it can be inverted by a polynomial least-squares fit, i.e.,

$$B = P_A(A_V, \psi) = \sum_i \sum_j a_{i,j} A_V^{i-1} \psi^{j-1}. \tag{14}$$

In a similar way, ψ can be expressed as a function of R_V and B through the equation

$$\psi = P_R(R_V, B) = \sum_i \sum_j r_{i,j} R_V^{i-1} B^{j-1}. \tag{15}$$

The upper values of i and j are typically 7 and 5 for P_A and P_R, respectively.

For a given model atmosphere, the coefficients for polynomials P_A and P_R can be computed and B and ψ can be recovered from any set of Stokes profiles through a very fast iterative loop,

$$B_n = P_A(A_V, \psi_{n-1}) \tag{16}$$

$$\psi_n = P_R(R_V, B_n), \tag{17}$$

initialized with $B_0 = 0$ and $\psi_0 = R_V$. The number of iteration steps is typically 3.

We do not discuss the determination of magnetic field azimuth ϕ, as it is detailed in Paper I; polynomial expansions of magneto-optical effects can be used to deduce directly ϕ from B, ψ, and Stokes Q and U.

7. Polynomials $P_D(B, \psi)$: inversion for an unknown model atmosphere

For a given model atmosphere, the differences D_V can be expanded as functions of B and ψ, i.e.,

$$D_V = P_D(B, \psi) = \sum_i \sum_j d_{i,j} B^{i-1} \psi^{j-1}. \tag{18}$$

The upper values of i and j are typically 5.

We performed simulations for four model atmospheres: FALA, FALC, FALF, and MALTM. They show that S_V , R_V, and D_V are very similar for models FALC, FALA, and FALF. Details are given in Sect. (14). As a consequence, the accuracy

of the inversion process is not degraded by selecting two models, for example, FALC and MALTM, and by interpolating inversion coefficients between both. For any set of V, Q, and U profiles, we define an interpolation coefficient δ_V in the following way:

$$\delta_V = \frac{D_V - P_{D,\mathrm{FALC}}(B,\psi)}{P_{D,\mathrm{MALTM}}(B,\psi) - P_{D,\mathrm{FALC}}(B,\psi)}. \quad (19)$$

If

$$\delta_V < -2 \quad (20)$$

or

$$\delta_V > 3, \quad (21)$$

the inversion process is given up for the corresponding solar pixel. This may occur for small Bf products mainly because of noise. We see later (Figs. 11 and 13) that very few points are involved.

We replace $S_{0,M}$ and polynomials P_A and P_R, defined in Sects. 5 and 6, by

$$S_{0,M} = (1-\delta_V)S_{0,\mathrm{FALC}} + \delta_V S_{0,\mathrm{MALTM}} \quad (22)$$
$$P_A = (1-\delta_V)P_{A,\mathrm{FALC}} + \delta_V P_{A,\mathrm{MALTM}} \quad (23)$$
$$P_R = (1-\delta_V)P_{R,\mathrm{FALC}} + \delta_V P_{R,\mathrm{MALTM}}. \quad (24)$$

Inside the iteration loop (Eqs. (16), (17)) we introduce Eqs. (18)–(24).

8. Broadening function for instrumental effects in SOT/SP data

We analyze SOT/SP data of the active region NOAA10958 observed on 17 May 2007 at 13:01 UT. The SOT/SP instrument (Lites et al. 2013) of the Solar Optical Telescope (Tsuneta et al. 2008) is on board the Hinode mission (Kosugi et al. 2007). Stokes profiles and level 2 outputs from inversions using the HAO "MERLIN" inversion code developed under the Community Spectro-polarimetric Analysis Center are available online[2].

As in any set of observations, a damping function can be used to mimic instrumental effects and to adjust synthetic profiles to observed data. In the case of unresolved solar structures, an additional effect should be taken into account. Across the same pixel, transverse gradients of the magnetic field may occur and, thereby, broaden Stokes profiles, especially for strong magnetic fields.

Figure 4 shows an example of observed V-profile (stars) corresponding to 2500 G (according to UNNOFIT inversion) together with the synthetic MALTM profile (dashed lines). The observed profile is clearly wider than the synthetic profile. It is approximately matched by the synthetic MALTM profile (full line) broadened with the Lorentz function plotted in Fig. 5 and corresponding to the damping coefficient $\gamma = 3$ pm.

To find a unique broadening coefficient that is valid for all data, we turned to the inversion results obtained from UNNOFIT and MERLIN codes. The value $\gamma = 3$ pm appears to produce a very good agreement in both cases inside a wide magnetic field range corresponding to filling factors close to 1, as we show in Figs. 14 and 17. All further calculations use that damping coefficient.

[2] http://www.csac.hao.ucar.edu/

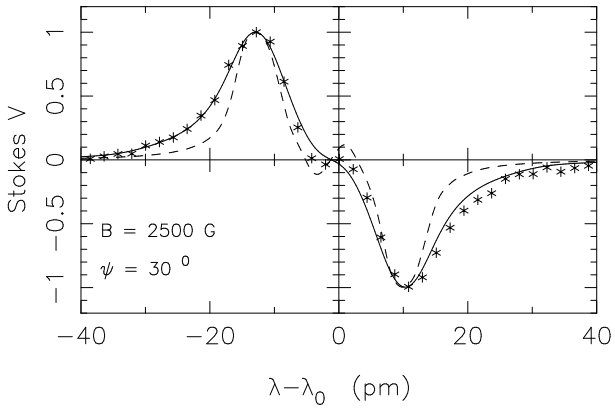

Fig. 4. V-profile from SOT/SP data (stars) for magnetic field strengh 2500 G. Normalized synthetic profiles are plotted for MALTM with (full lines) and without (dashed lines) additional broadening.

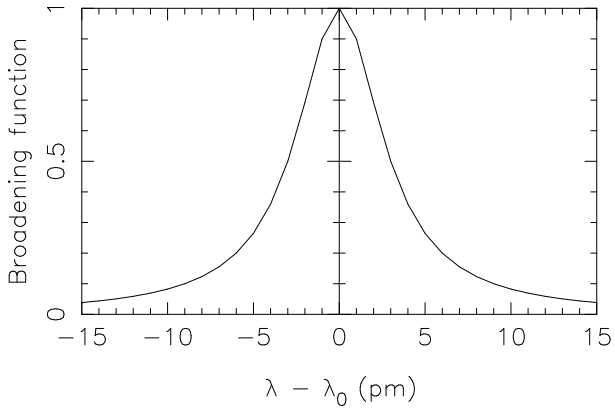

Fig. 5. Lorentz broadening function for synthetic V-profiles.

The μ value is near 0.90, close to 1. We can also note that the use of a broadening function automatically adjusts the profile widths to the widths corresponding to the μ value of observations. So, before broadening, we can use synthetic profiles at disk center.

Using a single coefficient to correct instrumental effects, model fitting, magnetic unresolved fluctuations, and center-to-limb effects is obviously a crude approximation. Further detailed investigations are needed, especially for future data exhibiting even higher resolutions and even lower noise levels. We return to this question in Sect. 15.

9. VMI inversion and model atmosphere selection

The synthetic functions S_V, R_V, D_V, and A_V corresponding to models FALC and MALTM are shown in Figs. 6 and 7.

For a given solar point, the calculation of A_V through Eq. (13) is possible only if $S_V > S_{0,M}$, where M stands for the model atmosphere that must be selected. We start the iteration by using the δ_V value that corresponds to the model MALTM providing the lowest $S_{0,M}$ value. By starting with the MALTM function we avoid eliminating some points of low magnetic field strengths.

The steps of the inversion are the following:

1) Initialization:
Computation of S_V,R_V,D_V

$B_0 = 0$

$\psi_0 = R_V$

$\delta_{V,0} = 1.$

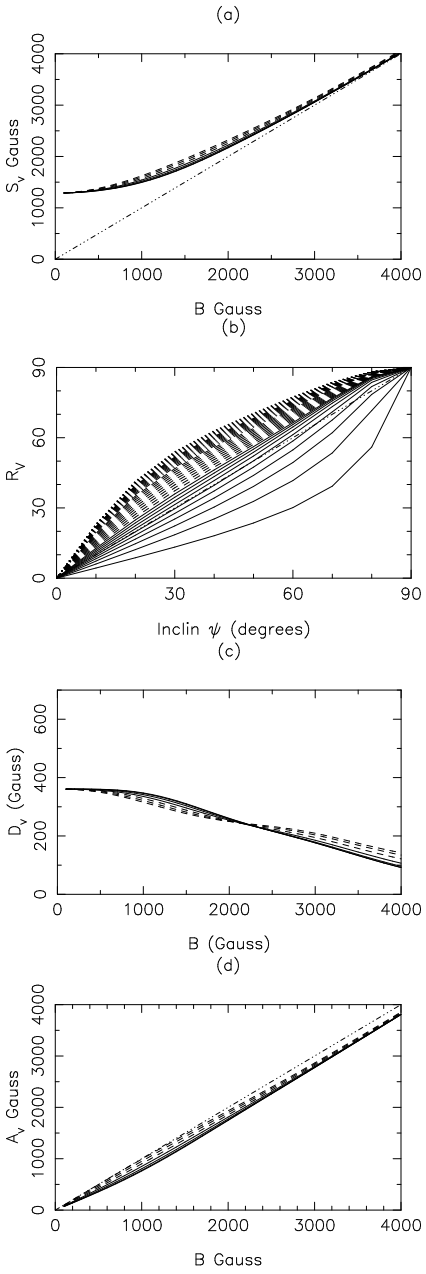

Fig. 6. S_V, A_V, D_V, and A_V functions for FALC model with additional broadening (Sects. 8, 9).

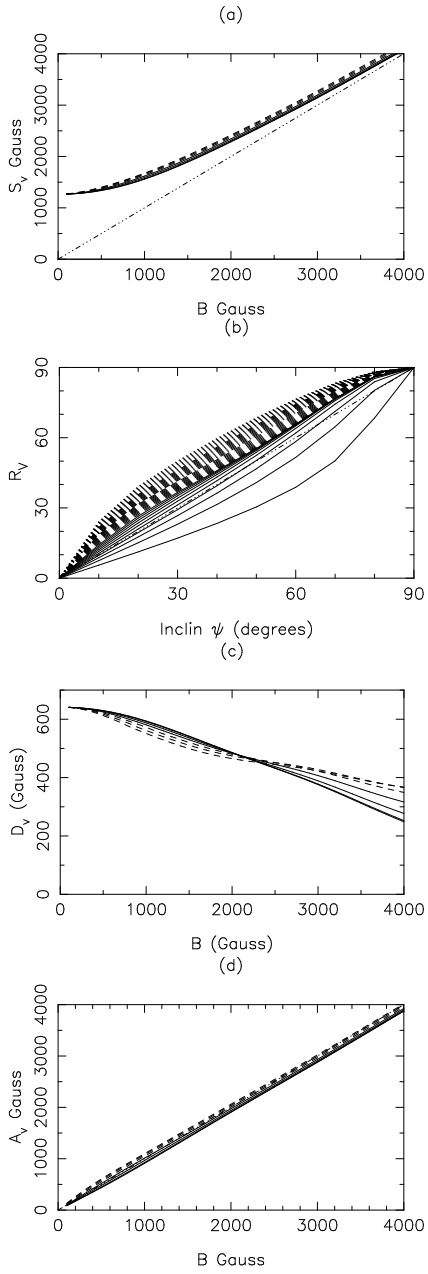

Fig. 7. S_V, A_V, R_V, and D_V functions for MALTM model with additional broadening.

2) Iteration step n (n = 1, 2, 3):

Eq. (22) $\rightarrow S_{0,M,n}$

Eq. (13) $\rightarrow A_{V,n}$

Eqs. (18)−(24) $\rightarrow \delta_{V,n}$, $P_{A,n}$,$P_{R,n}$

Eqs. (14), (15) $\rightarrow B_n$, ψ_n

10. SOT/SP data: Estimates and reduction of noise effects

10.1. Data noise level

As mentioned in Sect. 4.2, we can estimate noise levels in Stokes parameters using RMS values ϵ over two wavelength intervals: at the beginning and the end of the available spectrum, where Q, U, and V are negligible.

Figure 8 shows results obtained across the full set of SOT/SP data with two 5 point intervals corresponding roughly to $-52 < \Delta\lambda < -42$ pm and $42 < \Delta\lambda < 52$ pm, where $\Delta\lambda$ is the wavelength distance from line center. To disentangle results from small and large magnetic fields B or filling factors f, we plot the results versus the product $B_U f_U$ deduced from UNNOFIT inversion. We note that UNNOFIT and MERLIN inversions lead to almost the same results insofar as the product Bf is concerned (see Sect. 12, Fig. 16). The values are normalized by the continuum intensity of quiet Sun I_Q, obtained by averaging continuum intensities over pixels such that $B_U f_U < 20$ G. Results are presented with circles for Q, triangles for U, and squares for V.

For $B_U f_U < 1000$ G, Q, U, and V decrease strongly for $|\Delta\lambda| > 42$ pm and ϵ/I_Q is close to 1.2×10^{-3}.

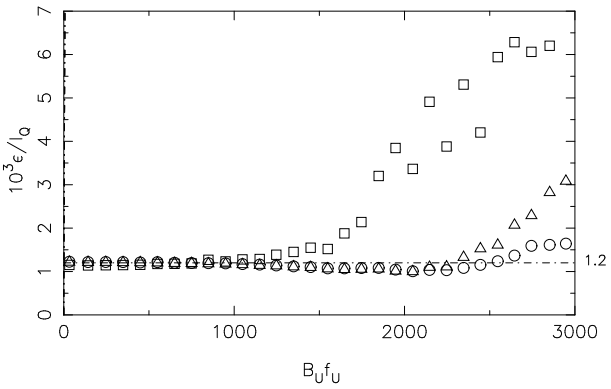

Fig. 8. RMS of Stokes profiles in far wings of the 630.2 nm line ($|\Delta\lambda| > 0.042$ nm) in SOT/SP data, divided by the quiet Sun continuum intensity, for noise level determination. Circles for Q, triangles for U, and squares for V.

10.2. Noise effects reduction for R_V computations

According to Fig. 8, ϵ/I_Q remains very near 1.2×10^{-3} for $B_U f_U < 2500$ G for Q and U. This shows that Q and U remain negligible in both 5-point wavelength intervals in a very wide magnetic field range. As mentioned in Sect. 4.2, for each pixel, we subtract from Q^2 and U^2 the average values over the two 5-point intervals to reduce noise effects on the R_V expression (7). Of course, more accurate results would be obtained with observations including a larger line profile that allows larger intervals.

10.3. Expected noise effects on VMI inversion

We use the $1.2 \times 10^{-3} I_Q$ noise level to predict effects on VMI inversion results. We can assimilate the continuum intensity to the quiet Sun continuum I_Q for synthetic FALC profiles.

However, the ratio between synthetic continuum level intensities of FALC and MALTM is very small, i.e.,

$$I_{C,\mathrm{MALTM}}/I_{C,\mathrm{FALC}} = 0.126, \tag{25}$$

mainly because of temperature differences between both model atmospheres. Moreover, for unresolved structures, we must take into account a geometrical filling factor f.

Therefore, to simulate data noise effects, we introduce the stochastic noise at the RMS level of 1.2×10^{-3} relative to the continuum intensity in the FALC model in synthetic profiles FALC and MALTM. Because the noise effects depend only on the signal-to-noise ratio, we keep the local continuum (FALC or MALTM) as a reference, but we divide this level by 0.126 for MALTM and by f if the filling factor is not 1. Of course, different stochastic values are added to quantities Q, U, and V for the same point.

We can see expected errors and the RMS of departures in B and ψ in Figs. 9 and 10 for the FALC and MALTM models, with filling factors 1 and 0.1 for FALC, and 1 and 0.7 for MALTM. Triangles mean that owing to noise, B and ψ computations are not always possible in the useful range, mainly because of observed values of S_V that are too low.

For inversion of magnetic strengths (upper plots), errors are small in the case of the FALC model and in the MALTM model for $f = 1$. They are larger for MALTM model if $f = 0.7$ and $B < 1400$ G. In all of the cases, however, errors on B decrease strongly for large magnetic fields. Mean expected ψ errors (lower plots) are computed in the range $500 < B < 4000$ G. They are reduced by noise subtraction from Q^2 and U^2 integrals (Sect. 4.2).

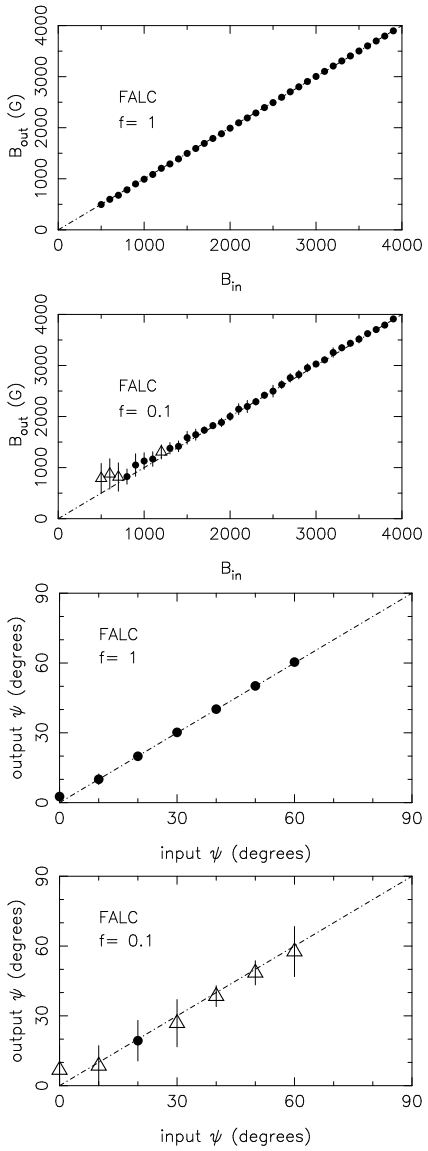

Fig. 9. Inversion of synthetic FALC model data for the case of data noise for filling factors 1 and 0.1.

11. Comparison between VMI and UNNOFIT results

We discuss now the results of VMI inversion of SOT/SP data, notably B_V and ψ_V. We compare them to results of UNNOFIT inversion (Landolfi et al. 1984; Bommier et al. 2007), namely B_U and ψ_U. The range of magnetic strengths is limited by the condition $S_V < 4500$ G, corresponding roughly to $B_V < 4000$ G. For very large magnetic fields, V-profiles cannot be neglected outside the available wavelength range (±52 pm). Additional inversion processes should be developed, for example, using V-profile extrapolations or maximum value determinations.

Most of the comparisons are presented versus the product $B_U f_U$. Indeed, because unresolved structures prevail with similar B values at low magnetic fluxes, $B_U f_U$ is a good criterion to disentagle ranges of quiet Sun, faculae, and spot penumbrae. Mean values are plotted with a 100 G step in the case of a number of values higher than 10 in each step. Dispersion is materialized by error bars.

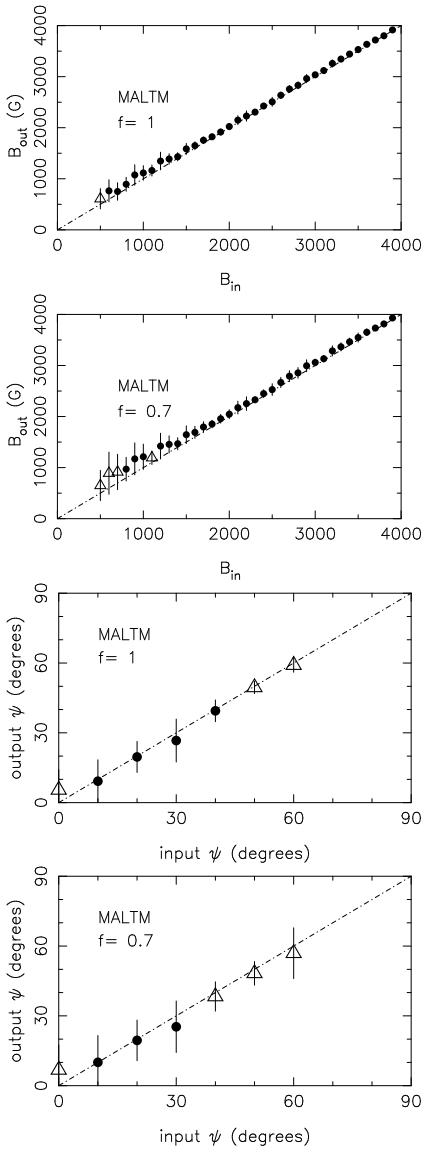

Fig. 10. Inversion of synthetic MALTM model data for the case of data noise for filling factors 1 and 0.7.

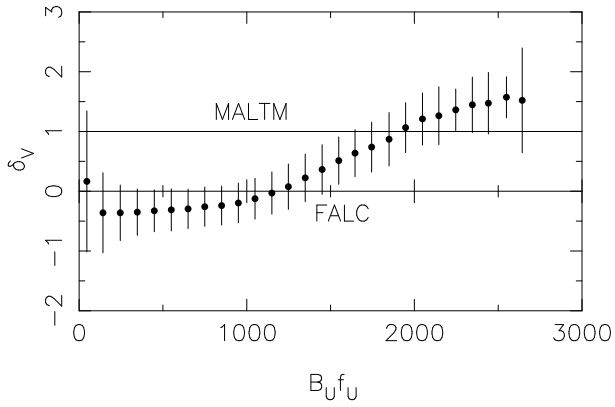

Fig. 11. SOT/SP data: δ_V versus UNNOFIT product $B_U f_U$.

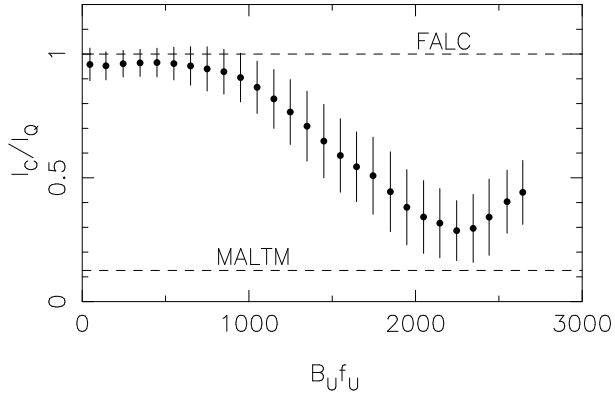

Fig. 12. SOT/SP data: continuum intensity versus UNNOFIT product $B_U f_U$.

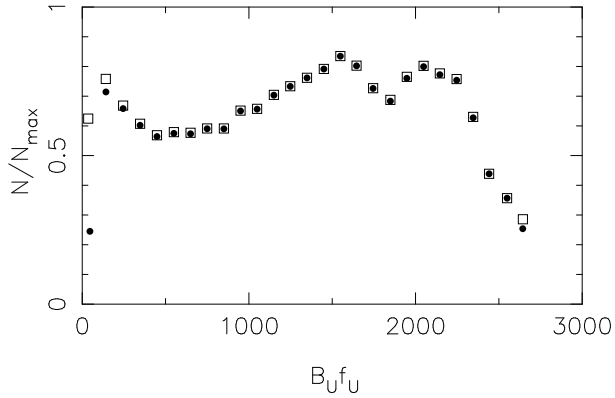

Fig. 13. Numbers of pixels so that $\psi_U < 60°$ or $\psi_U > 120°$ (squares) and numbers of pixels computed by VMI (black points) divided by the total number of available pixels in UNNOFIT inversion.

11.1. Model selection and the δ_V coefficient

Figure 11 indicates the plot of δ_V versus the product $B_U f_U$, in the range of inclination angles $0 < \psi_U < 60°$ and $120° < \psi_U < 180°$. Mean values are black points and the RMS of departures are indicated with vertical lines. Equations (20) and (21) imply $-2 < \delta_V < 3$. The standard deviations, however, are generally smaller than 0.5, which show that very few points are lost because of this constraint.

We see that, in the range $200 < B_U f_U < 1000$ G, δ_V is near 0 (FALC), while for higher values it increases up to 1 or more for spot umbrae (MALTM). This shows that the criterion D_V, which is only the difference between widths of V- and V^2-profiles, provides an estimate of the model atmosphere selection between FALC and MALTM, and that these two models together match well the whole set of data by representing two extreme cases.

In Fig. 12 we plot the ratio between continuum intensity I_C and continuum quiet Sun intensity I_Q that is obtained by averaging pixels defined by $B_U f_U < 20$ G. As expected, this ratio, close to 1 in the range $B_U f_U < 1000$ G, decreases down to 0.3 for $B_U f_U > 2000$ G. The discrepancy with the expected MALTM value 0.126 may be due to scattered light.

11.2. Validity range of VMI inversion for SOT/SP data

Figure 13 shows the number N of available solar pixels divided by the total number of pixels $N_{\max}$ (when $N_{\max} > 10$) in two different assumptions. Squares correspond to pixels where $\psi_U < 60°$ or $\psi_U > 120°$ and black points to pixels available in VMI inversion. We see that black points are well centered in the corresponding squares, except for very large fields ($B_U f_U > 2600$ G) or points such that $B_U f_U < 200$ G.

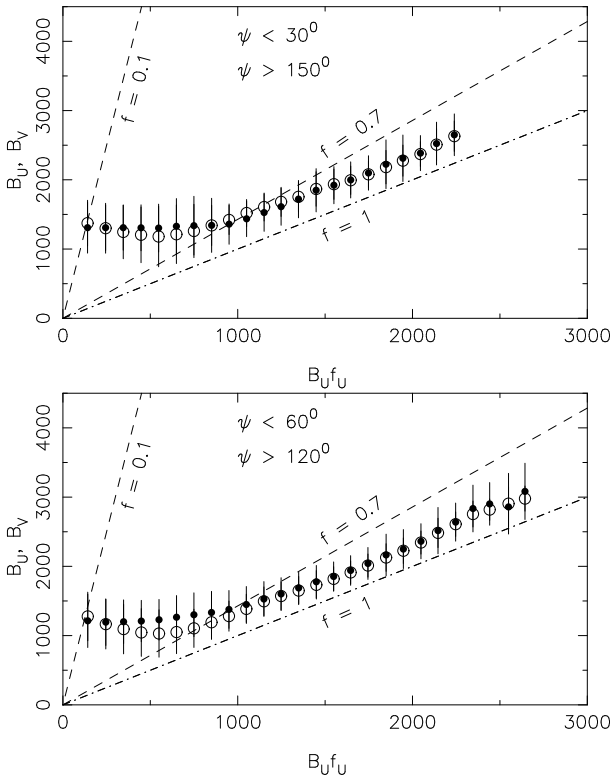

Fig. 14. Magnetic strengths from VMI inversion (black points) and UNNOFIT inversion (circles) in the ranges $0 < \psi_U < 30°$ and $150° < \psi_U < 180°$ (*top*) and $0 < \psi_U < 60°$ and $120° < \psi_U < 180°$ (*bottom*).

Below this limit, lost pixels correspond generally, either to effects of noise lowering S_V values or to the fact that the assumed atmospheric model of magnetic areas is not valid so that the lowest S_V value of the model is higher than the observed value. The relative numbers of lost pixels correspond to the departures between the centers of squares and black points. They are very small for $200 < B_U f_U < 300$ G and practically zero for $300 < B_U f_U < 2600$ G.

11.3. Magnetic field strengths B

In Fig. 14, we plot B_V (black points) and B_U (circles) for $B_U f_U > 100$ G. Each field strength corresponds to an average value across a 100 G $B_U f_U$ interval including more than 10 pixels. Vertical lines indicate RMS of departures. The data are restricted to points where $\psi_U < 30°$ or $\psi_U > 150°$ (upper diagram) and $\psi_U < 60°$ or $\psi_U > 120°$ (lower diagram). Dashed lines indicate limits corresponding to filling factors f_U equal to 1, 0.7, and 0.1, corresponding to values used in Sect. 10 to estimate noise effects.

To discuss the validity of VMI results in spite of noise effects, we assume that f_U values are near the ratio between magnetic and nonmagnetic areas inside each pixel. We consider three cases:

(a) In the range $200 < B_U f_U < 1000$ G, Fig. 11 shows that magnetic areas are mainly relevant to the FALC model. Because all B_V computed values are generally higher than 1000 G with $f > 0.1$, results appear to be reliable according to Fig. 9. We can note that if the noise level was reduced by a factor 2, Fig. 9b would apply to the filling factor $f = 0.05$. Then Fig. 14 shows that all values such that $B_U f_U > 100$ G would become reliable.

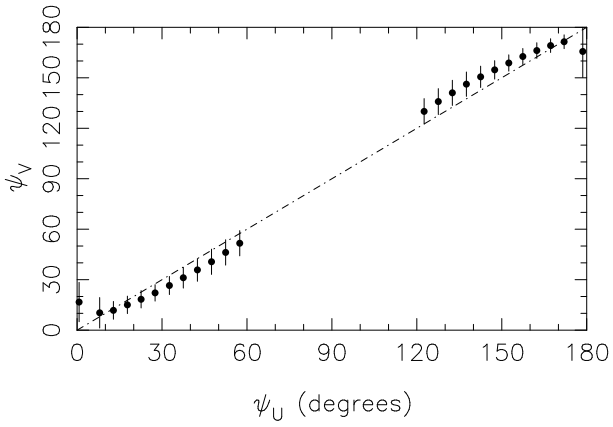

Fig. 15. Inclinations from VMI versus UNNOFIT.

(b) In the range $1000 < B_U f_U < 2000$ G, all B_V values correspond approximately to $f > 0.7$ with $B_V > 1000$ G, which indicates reliable results for the FALC model and approximate results for MALTM model, according to Figs. 9 and 10. Anyway, they are in good agreement with B_U values.

(c) For higher magnetic fields, some VMI results are a little larger than UNNOFIT results. The magnetic model with only one value of magnetic field is perhaps not relevant to such strong fields. Because VMI uses moments of $V \times |V|$ that are less sensitive to noise than moments of V, departures can be due to the different weights assigned to different parts of the profiles. We can expect that magnetic field transverse gradients, which are larger for strong fields than for weak fields, account for observed discrepancies, increasing with magnetic fields. As for the MISMA code, more complex models, including more than two columns or vertical and horizontal gradients and asymmetries, might be investigated.

11.4. Inclinations ψ

In Fig. 15 we plot inclinations from VMI inversion versus UNNOFIT results in the range $B_U f_U > 200$ G. As expected, the relative behavior of the results is opposite for angles symmetrical versus 90°. We restrict the discussion to $\psi < 90°$. We can see from Figs. 6 and 7 that for a given R_V value, ψ decreases when B increases. Because VMI B values are a little higher than UNNOFIT values in some ranges, as we show in Fig. 14 (bottom), we may expect ψ_V to be somewhat lower than ψ_U, as it is observed. However, for low ψ values, noise effects still appear to be present in spite of the correction mentioned in Sect. 4.2.

12. Comparison between VMI and MERLIN results

12.1. Magnetic field strengths B

Figure 16 shows that, as expected, $B_M f_M$ products, extracted from the MERLIN inversion, are very similar to $B_U f_U$ products used in Sect. 11.

Magnetic field strengths from VMI and MERLIN inversions are plotted in Fig. 17 as functions of $B_M f_M$ in the ranges $0 < \psi_M < 60°$ and $120° < \psi_M < 180°$. Three cases can be considered again:

(a) In the range $B_M f_M < 700$ G, VMI values are higher, especially for very low $B_M f_M$. Departures are simply because MERLIN code deals with stray light effects, but not with unresolved structures.

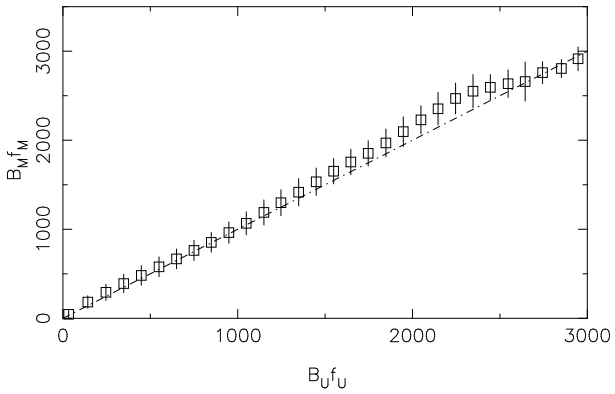

Fig. 16. Bf products from MERLIN inversion versus Bf products from UNNOFIT inversion.

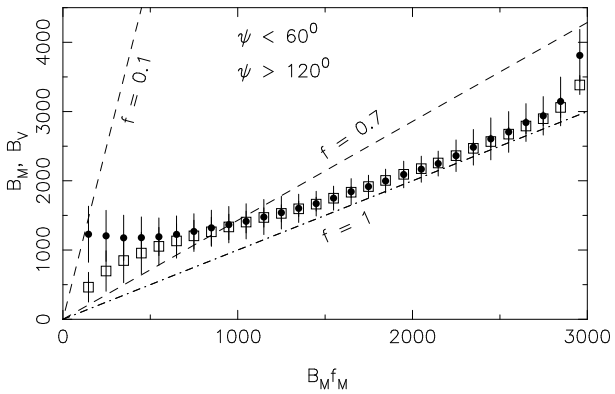

Fig. 17. Magnetic strengths from VMI (black points) and MERLIN inversion (squares) versus $B_M f_M$ values in the ranges $0 < \psi_M < 60°$ and $120° < \psi_M < 180°$.

(b) For $700 < B_M f_M < 2000$ G, the agreement is good. It can be noted also that the dispersion of B is very small for each $B_M f_M$ value.
(c) For $B_M f_M > 2000$ G, VMI values appear to be a little higher than MERLIN values, especially for very large magnetic fields. As in Sect. 11.3, we can note that unresolved transverse magnetic field gradients, increasing with magnetic strengths, may account for the observed discrepancies.

12.2. Inclinations ψ

Inclinations are plotted in Fig. 18 in the range $B_M f_M > 200$ G. They are in rather good agreement with MERLIN results, even for small inclinations.

13. VMI quick-look without iteration

As we show in Figs. 6a and 7a, S_V values are similar for FALC and MALTM for instrumental broadening, especially for small magnetic strengths. So we can try to replace the interpolation between both basic models by a mean model atmosphere. Moreover, we can use a further simplification by suppressing iterations and replacing curves A_V and R_V by the first bisector in plots (b) and (d) of Figs. 6 and 7, to get a so-called quick-look VMI ignoring the coupling between B and ψ. It can be noted indeed that R_V is close to ψ especially for B values near 1000 G, that is, in the full range $B_U f_U < 1000$ G.

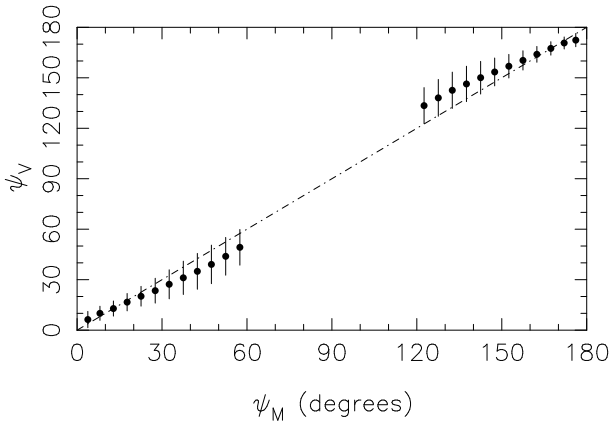

Fig. 18. Inclinations from VMI versus MERLIN inversion code.

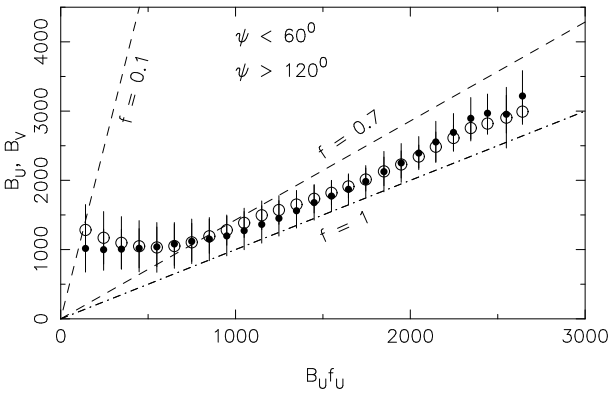

Fig. 19. Same caption as for Fig. 14 (bottom), but for VMI quick-look without iteration. Magnetic strengths from VMI inversion (black points) and UNNOFIT inversion (circles) in the ranges $0 < \psi_U < 60°$ and $120° < \psi_U < 180°$.

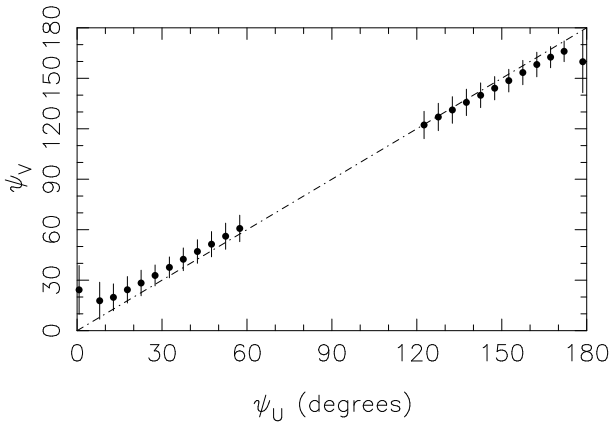

Fig. 20. Same caption as for Fig. 15, but for VMI quick-look without iteration.

Because we know the broadening function and the mean values S_{V0} of S_V for FALC and MALTM near $B = 0$, we can reduce the inversion to two equations

$$B = A_V = (S_V^2 - S_{V0}^2)^{1/2} \tag{26}$$

and

$$\psi = R_V, \tag{27}$$

where S_{V0} is equal to the average between $S_{0,\mathrm{FALC}}$ and $S_{0,\mathrm{MALTM}}$.

Results plotted in Fig. 19 are not very different from results plotted in Fig. 14b in the range $200 < Bf < 2700$ G. This is a

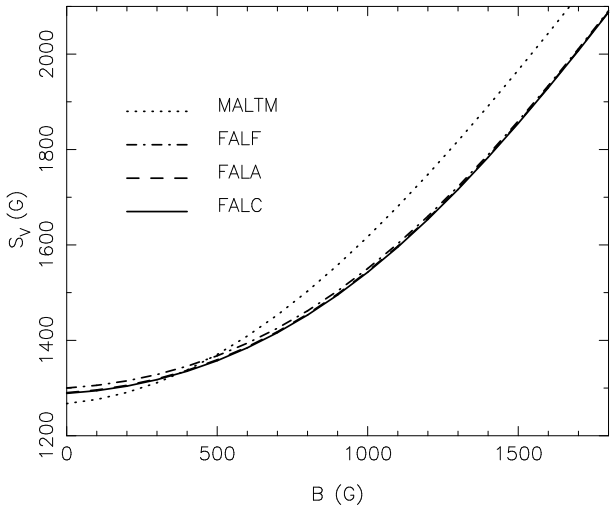

Fig. 21. Synthetic S_V values as functions of B for $\psi = 0$ and instrumental broadening $\gamma = 3$ pm for model atmospheres FALC, FALA, FALF, and MALTM. Curves correponding to FALC and FALA are almost superimposed (departures around 2 G).

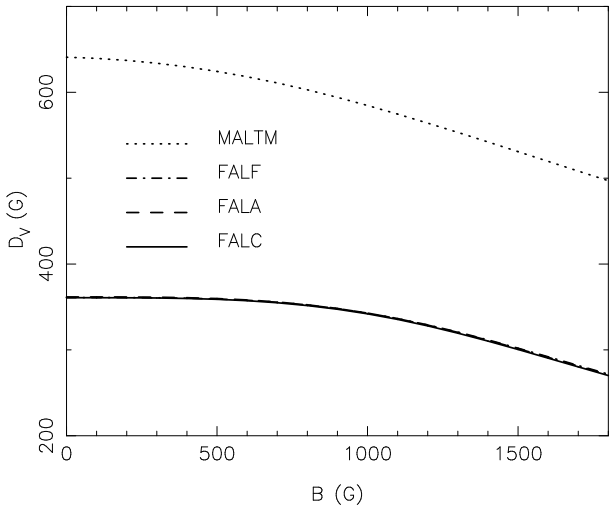

Fig. 22. Synthetic D_V values as functions of B for $\psi = 0$ and instrumental broadening $\gamma = 3$ pm for model atmospheres FALC, FALA, FALF, and MALTM. Curves correponding to FALC, FALA and FALF are almost superimposed (departures around 2 G).

clear indication of the small dependency of inversion results on the assumed model atmospheres.

14. Magnetic field strength dependency on model atmospheres

14.1. Synthetic S_V and D_V for four model atmospheres

As we show in Figs. 6a and 7a, S_V quantities deviate from B values especially in the weak field regime, so that inversion results are expected to depend more strongly from the assumed model atmospheres in this range. It is, therefore, interesting to estimate the accuracy of the full inversion process using D_V quantities and interpolations between model atmospheres.

Figure 21 shows synthetic S_V values as functions of B for instrumental broadening $\gamma = 3$ pm, as in Figs. 6a and 7a. Results from model atmospheres FALA and FALF were added to FALC and MALTM. For simplification, the plots are limited to low values of B with $\psi = 0$. Similarly, synthetic D_V values are plotted in Fig. 22, as in Figs. 6c and 7c.

According to the results from SOT/SP data (Fig. 14), the useful range of B magnetic strength is roughly $B > 1000$ G. In this range, we note that FALC, FALA, and FALF curves are almost superimposed. The S_V departures between FALC, FALA, and FALF are always smaller than 10 G, while departures between MALTM and FALC (or FALA and FALF) exceed 50 G. This shows that the accuracy of inversion results is practically not reduced by eliminating FALA and FALF from the interpolation process between FALC and MALTM.

14.2. Inversion of SOT/SP data in the range Bf > 1000 G

For observational data such as the SOT/SP data, magnetic strengths (Fig. 14, top and bottom), depend only slightly on the range of inclination angles. We consider the most simple case of small inclinations $\psi_U < 30°$ and $\psi_U > 150°$, which also takes advantage of a higher signal-to-noise ratio. In Fig. 23, we plot the mean results of SOT/SP data VMI inversion with model interpolation between FALC and MALTM (black points) along with UNNOFIT results (circles), as in the top of Fig. 14. We add by comparison the curves noted Fγ (full lines) and Mγ (dotted lines)

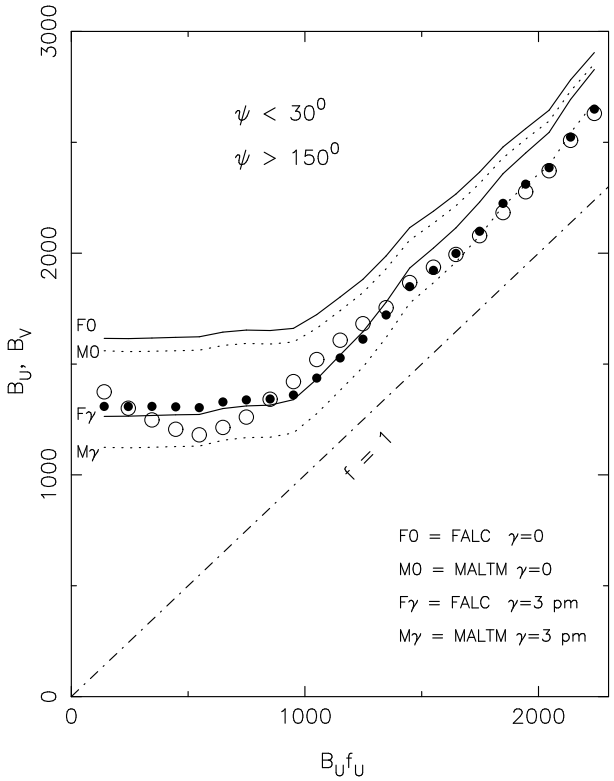

Fig. 23. Magnetic field strength output from UNNOFIT and VMI inversions (circles and black points, respectively). Full and dotted lines correspond to VMI inversions assuming only one given model atmosphere (F0 and M0 without instrumental broadening, Fγ and Mγ with broadening $\gamma = 3$ pm).

corresponding to results obtained by assuming only one model atmosphere, without interpolations, for FALC and MALTM, with the assumed instrumental broadening $\gamma = 3$ pm.

The VMI and UNNOFIT results behave similarly for $B_U f_U > 1000$ G. These results leave the Fγ line to reach the Mγ line, as is expected from the δ_V function plotted in Fig. 11. In the range $B_U f_U > 1300$ G, the use of a simple linear

interpolation (Eqs. (19)−(24)) leads to departures less than 50 G between VMI and UNNOFIT.

14.3. Inversion of SOT/SP data in the range $200 < Bf < 1000$ G

The agreement is a little less good in the range $B_U f_U < 1000$ G.

According to δ_V values (Fig. 11), FALC is roughly the best model atmosphere, so that results do not depend very much on the interpolation process. Moreover, although filling factors are small (around 0.15 for $Bf = 200$ G), we expect low data noise effects (even for $f = 0.1$, according to Fig. 9). However, we must remind ourselves that for small filling factors, we can expect departures between inversion methods that are using I-profiles or not.

It can be noted as well that inversion results using FALC and MALTM separately (curves Fγ and Mγ) lead to B values that are always higher than 1000 G in the range $Bf > 200$ G. According to Fig. 21, they correspond to S_V values higher than 1500 G and, therefore, much higher than S_0 for any of the four models FALC, FALA, FALF, and MALTM. We see also in Fig. 23 that departures between curves Fγ and Mγ never exceed 150 G. This accounts for the relatively small dependency on model atmospheres in this range.

14.4. Prospects for a better model selection

To improve the model selection, further investigations are necessary to provide a better understanding of the relationship between thermodynamical parameters and the shape of V-profiles. More specifications might be extracted from additional measurements based not only on differences between lobe shifts of V- and V^2-profiles. They would permit the use of nonlinear interpolation between more than one parameter and more than two model atmospheres. The magnetic strength itself might be included in atmosphere specifications during the iteration process. We return to the possibility of new simulations of unresolved magnetic flux tubes through 3D-MHD simulations in Sect. 16.

15. Magnetic field strength dependency on instrumental broadening

In Fig. 23 we also plotted the mean results of SOT/SP data inversions without model interpolation for the FALC and MALTM models, but this time without instrumental broadening ($\gamma = 0$). They are noted F0 and M0.

The resulting mean magnetic strengths B are always larger than 1500 G. Because values that are too high are obtained in both cases, we assumed that the error was not due to model atmospheres, but mainly to instrumental broadening. The γ coefficient is adjusted to get the best agreement with UNNOFIT and MERLIN results especially in the range $Bf > 1000$ G, where filling factors are close to 1 and where disturbances due to mixing between magnetic and nonmagnetic spectra do not affect I-profiles.

Of course, it would be better in the future to get direct estimates of instrumental effects to check whether the perceived broadening is not in part due to the assumed model atmospheres.

16. Stokes V amplitude and filling factors

In the weak field approximation, the Bf products and, more generally, the magnetic flux in the line-of-sight direction can be deduced approximately from the maximum Stokes V amplitude by

$$Bf \cos\psi = 0.21 \times 10^{12} \frac{\Delta\lambda_D}{\lambda_0^2 \overline{g}} \frac{|V|_{max}}{I_C - I_0}, \quad (28)$$

according to Landi Degl'Innocenti et al. (2004) and Bommier et al. (2009). The parameter λ_0 is the line wavelength in nm, $\overline{g}$ the effective Lande factor, $\Delta\lambda_D$ the Doppler width, and $I_C - I_0$ the difference between continuum and line center intensity in magnetic areas.

For very small filling factors, the observed continuum, line center intensity, and Doppler width correspond to the spectrum of nonmagnetic areas, outside magnetic flux tubes. However, $I_C - I_0$ decreases approximately by a factor 8 between the extreme cases of FALC and MALTM (Sect. 10.3), while $\Delta\lambda_D$ decreases by a much smaller factor. Hence, assuming the same model atmosphere inside and outside magnetic areas may lead to errors on determinations of $Bf \cos\psi$ and filling factors f.

The same problem may also arise in the general case of any magnetic strength for inversions using the same thermodynamical parameters in magnetic and nonmagnetic areas. Further investigations might be able to connect flux tube model atmospheres more accurately with various moments (barycenters and widths) of V-profiles. This should lead to more accurate values of filling factors and magnetic fluxes.

Such investigations could be carried out with synthetic polarization profiles obtained from realistic 3D-MHD simulations of the solar photosphere obtained, for example, from the MURaM code (Vögler et al. 2005). These simulations would allow us to estimate and model the effect of unresolved magnetic structures on the observed V-profile shapes (see Shelyag et al. 2007). With that prospect, a database giving access to synthetic Stokes spectra of the most commonly used magnetic sensitive lines, computed for various magnetic regimes from 3D-MHD simulations would be a very valuable tool for testing inversion methods.

17. Conclusions

VMI specificity and speed. The VMI inversion method can help to make progress in the analysis of unresolved structures by providing magnetic field vectors independently of I-profiles. It determines magnetic field vectors for inhomogeneous solar structures in the context of two-component solar models, i.e., magnetic and nonmagnetic. In the same way, results remain reliable if intensity profiles are disturbed by scattered light. The specific point is that VMI does not depend on any nonmagnetic component, since it is independent of the Stokes I profile.

The number of iteration steps typically does not exceed 3 and VMI iterations are very fast. The computing time is less than 3×10^{-4} s per pixel with a four-processor Xeon computer (8 cores, 2.4 GHz). The useful inclination range is typically $0 < \psi < 60°$ and $120 < \psi < 180°$. It might be complemented by Q-moments inversions for ψ angles around 90°.

Comparison with UNNOFIT and MERLIN inversions. SOT/SP data in the 630.2 nm FeI line have been processed.

Mean VMI B values are always higher than 1000 G and in rather good agreement with UNNOFIT results for $200 < Bf < 2000$ G. No really significant departures can be associated with differences between model atmospheres in magnetic and nonmagnetic areas (Sects. 1.2 and 11.3).

Mean VMI values are also in good agreement with MERLIN results for $700 < Bf < 2000$ G. In the range $Bf < 700$ G,

departures are present because unresolved structures are not included in the MERLIN code.

For very strong fields, VMI B values are slightly higher than those derived with UNNOFIT or MERLIN. Stokes profiles should probably be represented by more complex models with several columns or transverse gradients of magnetic field.

Model atmospheres. We emphasized the importance of model atmosphere selection from the shape of V-profiles in Sect. 14. This paper uses the simplest way to accommodate thermodynamical variation, namely with an interpolation between only two model atmospheres, using the difference between lobe shifts in V- and V^2-profiles. Relationships between thermodynamical parameters and shape of V-profiles might be investigated in more detail with new sets of theoretical 3D-MHD simulations

Line broadening and data noise effects: Possible improvements. The accuracy of results should be improved via a direct determination of the γ coefficient characterizing instrumental line broadening.

Data noise effects are already reduced in V-moments calculations with the use of $V \times |V|$ instead of V^2 (Sect. 4.1) and with noise subtraction in Q^2 and U^2 (Sect. 4.2). Estimates of errors (Figs. 9 and 10), however, show that some reduction of noise level should provide reliable B results for Bf values that are much lower than the present limit, which is approximately 200 G. A factor 2 should be sufficient to lower the limit down to 100 G.

Data noise might also be reduced by longer exposure times on the condition that spatial resolution is not degraded. Wider wavelength intervals across the line profile should also help, not only to increase the accuracy of high magnetic field measurements, but also to allow a better determination and a better correction of noise in the far wings of the line, where Stokes parameters are expected to be negligible.

Profiles of infrared lines, which are more sensitive to low magnetic fields because of larger Zeeman shifts, could also be investigated.

Acknowledgements. We thank the referee for fruitful comments. HINODE is a Japanese mission developed and launched by ISAS/JAXA, with NAOJ as domestic partner and NASA and STFC (UK) as international partners. It is operated by these agencies in cooperation with ESA and NSC (Norway). Hinode SOT/SP Inversions were conducted at NCAR under the framework of the Community Spectro-polarimtetric Analysis Center (CSAC; http://www.csac.hao.ucar.edu).

References

Asensio Ramos, A. 2009, APJ, 701, 1032
Bommier, V. 2011, A&A, 530, A51
Bommier, V., Landi Degl'Innocenti, E., Landolfi, M., & Molodij, G. 2007, A&A, 464, 323
Bommier, V., Martinez Gonzalez, M., Bianda, M., et al. 2009, A&A, 506, 1415
Bruls, J. H. M. J., & Trujillo Bueno, J. 1996, Sol. Phys., 164, 155
Criscuoli, S., Ermolli, I., Uitenbroek, H., & Giorgi, F. 2013, ApJ, 763, 144
Del Toro Iniesta, J. C., Orozco Suarez, D., & Bello Rubio, L. R. 2010, ApJ, 711, 312
Fontenla, J. M., Avrett, E. H., & Loeser, R. 1993, ApJ, 406, 319
Kosugi, T., Matsuzaki, K., Sakao, T., et al. 2007, Sol. Phys., 243, 3
Landi Degl'Innocenti, E., & Landolfi, M. 2004, Polarization in Spectral Lines (Dordrecht: Kluwer Acad. Publ.)
Landolfi, M., Landi Degl'Innocenti, E., & Arena, P. 1984, Sol. Phys., 93, 269
Lites, B. W., Akin, D. L., Card, G., et al. 2013, Sol. Phys., 283, 579
Maltby, P., Avrett, E. H., Carlsson, M., et al. 1986, ApJ, 306, 284
Mathys, G., & Stenflo, J. O. 1987, A&A, 171, 368
Mein, P., Uitenbroek, H., Mein, N., Bommier, V., & Faurobert, M. 2011, A&A, 535, A45
Orozco Suarez, D., Bellot Rubio, L. R., Del Toro Iniesta, J. C., et al. 2007, PASJ, 59, S837
Rybicki, G. B., & Hummer, D. G. 1991, A&A, 245, 171
Rybicki, G. B., & Hummer, D. G. 1992, A&A, 262, 209
Semel, M. D. 1967, Ann. Astrophys., 30, 513
Shelyag, S., Schüssler, M., Solanki, S. K., & Vögler, A. 2007, A&A, 469, 731
Skumanich, A., & Lites, B. 1987, ApJ, 322, 473
Solanki, S. K., Keller, C., & Stenflo, J. O. 1987, A&A, 188, 183
Stenflo, J. O. 1973, Sol. Phys. 32, 41
Stenflo, J. O. 2010, A&A, 517, A37
Tsuneta, S., Ichimoto, K., Katsukawa, Y., et al. 2008, Sol. Phys., 249, 167
Uitenbroek, H. 2001, ApJ, 557, 389
Uitenbroek, H. 2003, ApJ, 592, 1225
Viticchié, B., & Sánchez Almeida, J. 2011, A&A, 530, A14
Viticchié, B., Sánchez Almeida, J., Del Moro, D., & Berrilli, F. 2011, A&A, 526, A60
Vögler, A., Shelyag, S., Schüssler, M., et al. 2005, A&A, 429, 335